AIAA JOURNAL
Vol. 30, No. 9, September 1992

# Effects of a Leading-Edge Fillet on the Flow Past an Appendage-Body Junction

William J. Devenport,* Roger L. Simpson,† Michael B. Dewitz,‡ and Naval K. Agarwal§
*Virginia Polytechnic Institute and State University, Blacksburg, Virginia 24061*

**Oil-flow visualizations and pressure and velocity measurements are presented to demonstrate the effects of a leading-edge fillet on the flow of a turbulent boundary layer past an idealized appendage-body junction. The fillet, a large fairing in the corner between the appendage nose and body surface, modifies the flow in a way that is desirable in many applications. With the appendage at zero angle of attack, it eliminates leading-edge separation and thus the formation of a horseshoe vortex around the wing nose. It greatly improves the stability of the flow close to the junction and the nonuniformity of its wake. At nonzero angles of attack, the desirable effects of the fillet are reduced, apparently because of separation of the body boundary layer as it approaches the pressure side of the fillet.**

## Introduction

THIS work forms the second part of an experimental study of passive devices for altering the horseshoe vortex formed in the flow past an appendage-body junction. The junction in question is shown in Fig. 1. It consists of an unswept cylindrical appendage with an airfoil cross section mounted on a flat wall on which an otherwise two-dimensional equilibrium turbulent boundary layer is growing. Junctions of this type are found between the hull and sail of a submarine, between a strut and endwall in a duct, at the base of bridge piers, and in other practical situations. Flow past such junctions is dominated by the formation a horsehoe vortex contained within a region of separation adjacent to the appendage.

Several of the characteristics of the horseshoe vortex are undesirable in may applications. First, it is subject to intense large-scale low-frequency unsteadiness (termed bimodal unsteadiness) in the vicinity of the appendage nose. This can lead to the generation of unwanted vibration or noise. Second, because of its rotational motion, the horseshoe vortex tends to bring high-momentum freestream fluid into close contact with the wall and appendage surface. This results in an increase in surface shear stresses, drag, and heat transfer from the flow. Third, the streamwise legs of the vortex can persist far downstream of the appendage. Turbulence levels within them are generally greater than in the surrounding wake, and they may interfere with the operation of other devices downstream.

Ideally, a passive flow control device would eliminate the bimodal unsteadiness and reduce as far as possible the strength of the horsehoe vortex. The bimodal unsteadiness, as described by Devenport and Simpson,[1] is generated by the reversal of turbulent fluid as it impinges on forward-facing parts of the appendage. Depending on whether this fluid originates in the boundary layer or in the irrotational freestream, it recirculates in a different pattern. Large-scale changes in the flowfield thus occur at irregularly spaced intervals. The strength of the horseshoe vortex depends not only on the details of its formation in the nose region but also on the amount of skew-induced streamwise vorticity that it entrains as it develops downstream. The amount of streamwise vorticity available for entrainment is directly related to the magnitude of the angle through which the boundary layer is turned as it encounters the appendage.

In the first part of this study, described by Devenport et al.,[2] the effects of placing a constant radius circular fillet around the entire base of the appendage were studied. Unfortunately, this device did not modify the flow in a desirable way; it did not eliminate the bimodal unsteadiness, and it appeared to increase the size and strength of the vortex legs and their unsteadiness in the wake. It is clear that this fillet failed because it did not prevent leading-edge separation, and it increased the skewing of the boundary layer in the vicinity of the appendage nose.

A device with more promising characteristics is a large fairing in the corner between the appendage nose and wall upstream, of the type shown in in Fig. 2, which we shall refer to as a leading-edge fillet. Some experimental work on devices of this type has been done in the past by Kubendran et al.[3] and Sung et al.[4] Kubendran et al. studied the effects of two leading-edge fillets on the flow of a laminar boundary layer past an appendage with a NACA 0012 section. In the plane of symmetry of the appendage, the fillets (see the inset of Fig. 2b) had triangular profiles with leading edges swept at angles of 45 and 63 deg. Flow visualizations performed with the appendage at 0- and 8-deg angle of attack showed the 63-deg fillet to be best, eliminating leading-edge separation and considerably reducing the skewing of the boundary layer as it encountered the appendage. Consistent with this, velocity measurements made downstream of the appendage showed a significant reduction in the nonuniformity of the wake produced by the legs of the horseshoe vortex, suggesting a reduction in their strength. The 63-deg fillet was also used by Sung et al. They studied its effect on the flow of a turbulent approach boundary layer past appendages with NACA 0012 and NACA 0020 sections. Their experimental results, limited to a few velocity profiles measured downstream of the appendages, again suggest that a device of this type reduces the nonuniformity of the wake.

The purpose of this paper is to present measurements to demonstrate more completely the effects of adding a leading-edge fillet to the flow of a turbulent boundary layer past an appendage-body junction. The bimodal unsteadiness, the time-average structure of the flow around the appendage, and the nonuniformity and unsteadiness of the wake are all examined. The effects of angle of attack and approach boundary-layer thickness are also investigated.

Presented as Paper 91-0252 at the AIAA 29th Aerospace Sciences Meeting, Reno, NV, Jan. 7-10, 1991; received Jan. 14, 1991; revision received Feb. 27, 1992; accepted for publication March 2, 1992. 

*Assistant Professor, Department of Aerospace and Ocean Engineering. Senior Member AIAA.

†Jack E. Cowling Professor, Department of Aerospace and Ocean Engineering. Fellow AIAA.

‡Graduate Assistant, Department of Aerospace and Ocean Engineering.

§Research Associate, Department of Aerospace and Ocean Engineering. Senior Member AIAA.

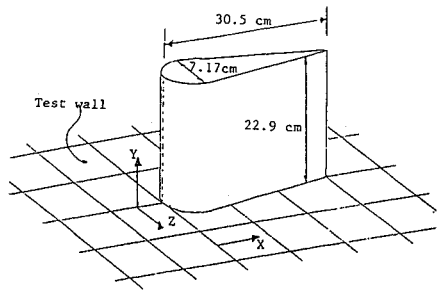


**Fig. 1 Baseline wing.**

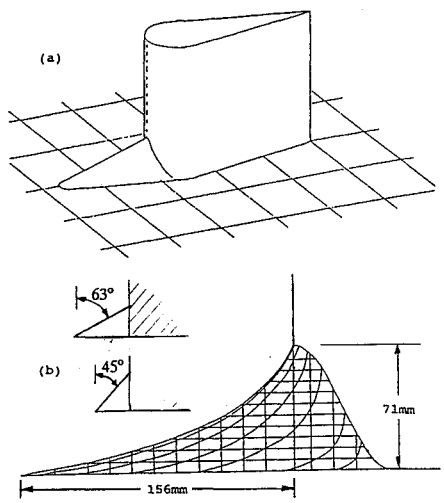


**Fig. 2 Wing with leading-edge fillet; a) perspective view, c) side view of leading-edge fillet. Inset b) shows configurations studied by Kubendran et al.[3]**

## Apparatus and Measurement Techniques

Only brief descriptions are given here, for more details see Devenport et al.[2] or Dewitz.[5]

### Wing Models

The two wing models used as appendages are shown in Figs. 1 and 2. Both were constructed from aluminum using a numerically-controlled milling machine. The baseline wing (Fig. 1) is cylindrical. Its cross section consists of a 3:2 elliptical nose (major axis aligned with the chord) and a NACA 0020 tail. It has a maximum thickness $T$ of 71.7 mm, a chord of 305 mm, and a span of 229 mm. The second wing (Fig. 2) is identical except for the addition of the leading-edge fillet. Unlike the devices studied by Kubendran et al. and Sung et al., the fillet was shaped to provide a smooth transition from the vertical surface of the wing nose to the horizontal wall upstream, since it was thought that this would improve its performance. The radius of curvature of the fillet surface is greatest on the chord line where it extends 156 mm upstream of the wing leading edge. The shape of the fillet was specified numerically by the David Taylor Research Center, Bethesda, Maryland.

For measurements at zero angle of attack, a boundary-layer transition trip, a 6.4-mm-wide strip of 120-grade sandpaper, was attached to both sides of the baseline wing 28.2 mm downstream of the leading edge. Surface oil-flow visualizations showed the trip to have no significant effect on the flow outside the wing boundary layer. No trips were used with the fillet.

### Test Conditions in Wind Tunnels

The two wing models were tested under a variety of conditions. A small boundary-layer tunnel (test section $0.91 \times 0.26 \times 6.0$ m) was used to examine the effects of the leading-edge fillet with the wing at zero angle of attack with two different approach boundary layers, to be referred to as the "thick" and "thin" boundary layers. The Virginia Tech Stability Wind Tunnel (test section $1.8 \times 1.8 \times 7.3$ m) was used for studies with the wing models at 0-, 6-, and 12-deg angle of attack. These studies were carried out with the thin approach boundary layer that was reproduced in this tunnel using a large flat plate. For measurements in this tunnel a cap was attached to the otherwise blunt top of the wing to avoid the complex flow that would otherwise be produced. The shape of the cap is that of a half-body of revolution generated by rotating the cross section of the wing about its chord line.

In both tunnels, blockage effects were minimal, freestream turbulence levels were low (less than 0.2%), and the approach boundary layers were closely two dimensional. The thick and thin boundary layers were produced with nominal approach freestream velocities of 27 and 32 m/s, respectively. Boundary-layer thicknesses, measured 2.15 wing thicknesses $T$ upstream of the baseline wing at zero angle of attack, were $0.50T$ and $0.26T$. These correspond to momentum-thickness Reynolds numbers of $6.6 \times 10^3$ and $4.5 \times 10^3$, respectively.

### Measurements Techniques

Oil-flow visualizations and mean surface pressure measurements were made on the wing models and surrounding wall. Visualizations were performed using a mixture of kerosine, titanium dioxide, and oleic acid using the procedure described by Maltby.[6] Where possible they were preserved (on a self-adhesive black plastic sheet applied to the model surfaces and test wall) using the method of Sutton,[7] described by Devenport and Simpson.[8] Mean surface pressures were measured through an array of static pressure taps using a scanivalve system and two Setra Model 230 transducers interfaced to an IBM AT computer.

**Table 1 Summary of measurements made with the baseline wing and the wing with leading-edge fillet.**

| Boundary layer: | Thick | Thin | Thin | Thin |
|---|---|---|---|---|
| Reynolds number, $Re$: | $6.6 \times 10^3$ | $4.5 \times 10^3$ | $4.5 \times 10^3$ | $4.5 \times 10^3$ |
| Angle of attack of wing, deg: | 0 | 0 | 6 | 12 |
| Oil-flow visualizations on test wall and wings | ✓ | ✓ | ✓ | ✓ |
| Mean surface pressures on test wall and wings | | ✓ | ✓ | ✓ |
| Hot-wire surveys of wake at $X/C = 3$ | ✓ | ✓ | ✓ | |
| LDV measurements near nose at $Z/T = 0$ | ✓ | ✓ | | |
| Microphone measurements in the nose region | ✓ | ✓ | ✓ | ✓ |
| in wake at $X/C = 3$ | ✓ | ✓ | ✓ | ✓ |

**Table 2 Uncertainty intervals calculated using the method of Kline and McLintock[13]**

| Quantity | Uncertainty |
|---|---|
| Mean pressure coefficient, $C_p$ | ± 0.006 |
| Mean velocity $U/U_e$, % | ± 2.8 |
| Turbulence normal stress $\bar{u}^2/U_{ref}^2$, % | ± 10.0 |
| location of hot wire, $T$ | ± 0.006 |
| $Z$ location of hot wire, $T$ | ± 0.05 |

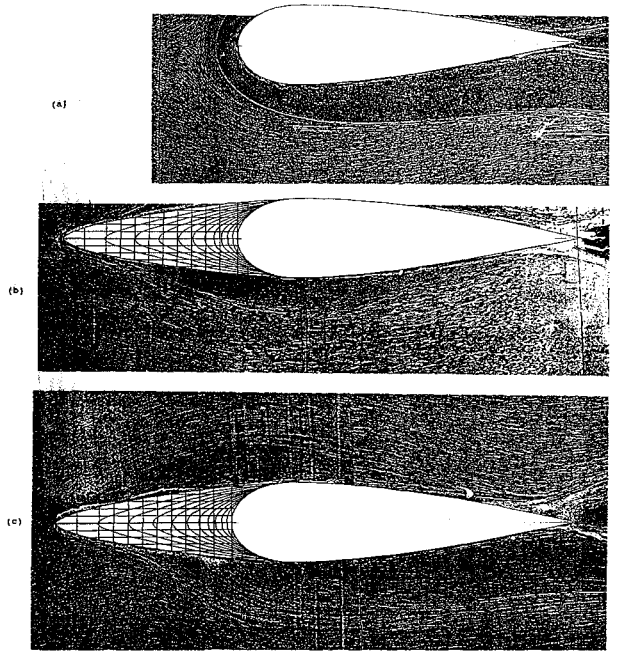

Fig. 3 Surface oil-flow visualizations on the test wall with the thin approach boundary layer; a) baseline wing, 0-deg angle of attack; b) wing with fillet, 0-deg angle of attack; c) wing with fillet, 12-deg angle f attack.

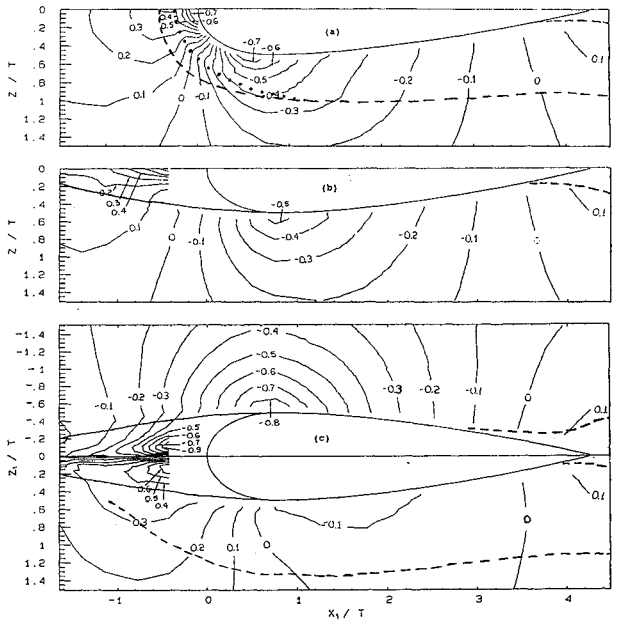

Fig. 4 Contours of mean surface pressure coefficient $C_p$ on the test wall and fillet surface with the thin approach boundary layer; a) baseline wing, 0-deg angle of attack; b) wing with fillet, 0-deg angle of attack; c) wing with fillet, 12-deg angle of attack. Solid lines show outlines of wing and fillet, dashed lines show separation lines seen in oil-flow visualizations, dotted lines show line of low shear.

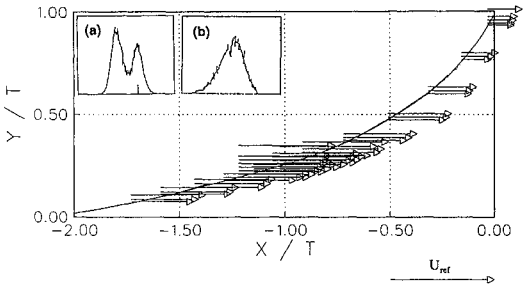

Fig. 5 Vectors of mean $U$-component velocity measured in plane of symmetry close to the fillet surface. Inset, histograms of velocity fluctuations, a) baseline wing, $X/T = -0.25$, $Y/T = .003$, $Z/T = 0$; b) wing with fillet $X/T = -1.1$, $Y/T = 0.226$, $Z/T = 0$. Zero angle of attack, thin boundary layer.

Hot-wire velocity measurements were made in the wakes using two rakes of 16 hot-wire sensors custom built by Dantec. These were operated using Miller[9] type constant-temperature anemometer bridges interfaced to the IBM AT. The rakes were calibrated in the wind tunnels against a pitot-static probe. To compensate for temperature variations in the stability wind tunnel (about 2–3 deg C/hour), the rakes were calibrated frequently and corrections, determined using Bearman's[10] method, were applied.

Surface pressure fluctuations were measured on the wall surrounding the wing models using Knowles Electronics BT1753 and Sennheiser MK10 microphones. The method of Agarwal and Simpson[11] (also described by Devenport et al.[2]) employing two closely spaced microphones was used to eliminate contributions to the microphone signals from vibration and acoustic noise.

Histograms of velocity fluctuations were measured upstream of the wing with fillet using part of the two-component laser-Doppler velocimeter (LDV) described by Simpson and Chew.[12] The aim here was to see if the leading-edge fillet eliminated the bimodal unsteadiness found around the nose of the baseline wing.

## Results

Results will be presented using the coordinate systems ($X$, $Y$, $Z$) and ($X_1$, $Y$, $Z_1$). The system ($X$, $Y$, $Z$), shown in Fig. 1, is fixed in the wind tunnel, the spanwise and streamwise coordinates $X$ and $Z$ being measured from a line coincident with the wing leading edge at zero angle of attack. The system ($X_1$, $Y$, $Z_1$) is fixed in the wing, $X_1$ and $Z_1$ being measured from the leading edge. In both systems $Y$ is measured normal to the test wall. Distances will be normalized on the maximum thickness of the wing $T$ or the wing chord $C$.

The measurements made are summarized in Table 1. Because of space limitations only a representative sample of the results are presented as figures. All of the results, however, are included in the following discussion. Uncertainties in measurements, calculated using the method of Kline and McClintock,[13] are listed in Table 2.

Examples of the surface oil-flow visualizations performed on the test wall surrounding the wing models are presented in Fig. 3. Major features appearing in these visualizations have been sketched in Fig. 4 along with corresponding contours of mean surface pressure coefficient $C_p$, which is defined as $(p - p_{ref})/(p_0 - p_{ref})$, where $p_0$ and $p_{ref}$ are the stagnation and static pressures of the approach freestream, and has an uncertainty of $\pm 0.006$. Note that Figs. 4b and 4c include pressure measurements made on the fillet surface as well as on the test wall.

LDV measurements of streamwise velocity component $U$ made close to the fillet surface in the plane of symmetry upstream of the appendage at zero angle of attack are presented in Fig. 5. Only results for the thin approach boundary layer are shown, since those for the thick boundary layer are qualitatively identical. Figure 5 also includes typical $U$-component velocity histograms measured with and without the fillet.

Hot-wire measurements of mean velocity $U$ and turbulence normal stress $\overline{u^2}$ made in a spanwise plane at $X/C = 3$ ($X/T = 12.7$) are presented as contours in Figs. 6 and 7. The $U$ and $\overline{u^2}$ are normalized on $U_{ref}$, the approach freestream velocity, and have uncertainties of $\pm 2.8$ and $\pm 10\%$, respectively. Note that with the wings at zero angle of attack measurements were made only on one side of the wake, the flow being assumed symmetrical. The complete cross sections shown in

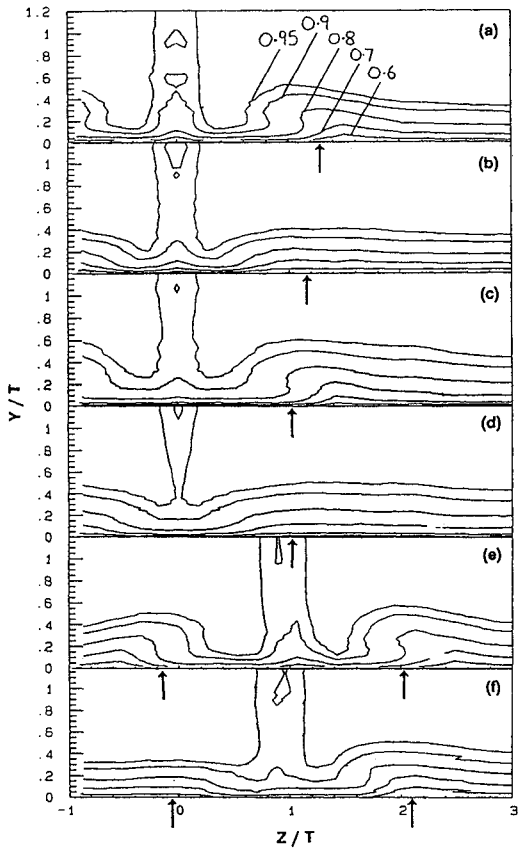


**Fig. 6 Contours of mean velocity $U/U_{ref}$ in the wake at $X/C = 3$; a) baseline wing, 0-deg angle of attack, thin boundary layer; b) wing with fillet, 0 deg thin; c) baseline wing, 0 deg, thick; d) wing with fillet, 0deg, thick; e) baseline wing, 6 deg, thin; f) wing with fillet, 6-deg, thick. Contour values shown in part a). Arrows on $Z$ axis mark locations of microphone measurements.**

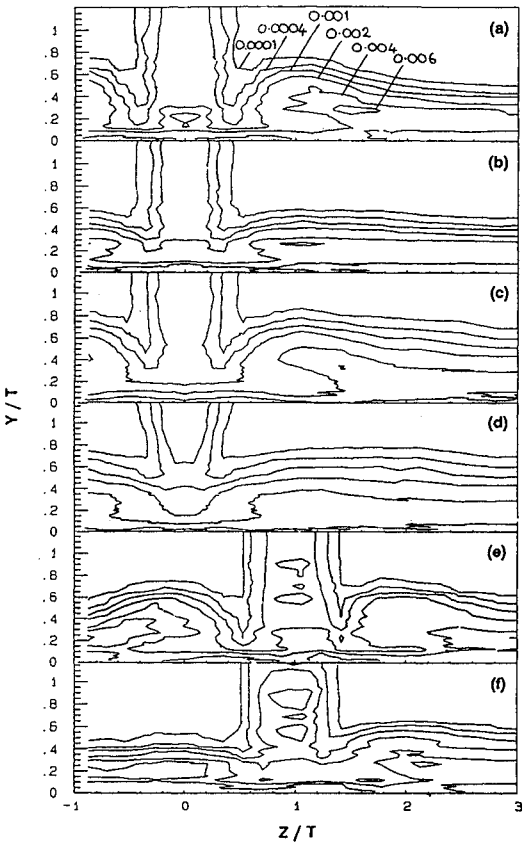


**Fig. 7 Contours of turbulence normal stress $\bar{u}^2/U_{ref}^2$ in the wake at $X/C = 3$; a) baseline wing, 0-deg angle of attack, thin approach layer; b) wing with fillet, 0 deg, thin; c) baseline wing, 0 deg, thick; d) wing with fillet, 0 deg, thick; e) baseline wing, 6 deg, thin; f) wing with fillet, 6 deg, thick. Contour values shown in part a).**

Figs. 6a–6d and 7a–7d were thus obtained by reflecting these data about $Z = 0$.

Surface pressure fluctuation spectra measured on the test wall to one side of the appendage nose (at $X/T = 0.27$, $Z/T = -0.748$) and in the wake of the appendage (at $X/C = 3$) are presented in Figs. 8 and 9, respectively. Measurements in the wake were made, as far as possible, underneath the apparent legs of the horseshoe vortex. Exact $Z$ locations are listed in Fig. 9 and where possible indicated by arrows drawn on the velocity contours of Fig. 6. For comparison, pressure spectra measured under the undisturbed two-dimensional zero-pressure gradient boundary layer produced at these locations with the appendage removed are included in Figs. 8 and 9. Note that all spectral levels and frequencies are normalized using $T$ and $U_{ref}$.

## Discussion

In the first part of this discussion, the characteristics of the flow past the baseline wing, at zero angle of attack with the thin boundary layer (the baseline case), will be described in the light of the present and previously published results. The effects of the leading-edge fillet on this flow will then be evaluated. Finally, the influences of boundary-layer thickness and angle of attack on the flow structure and efficacy of the fillet will be addressed.

### Baseline Case

Much of the time-average structure of this flow is visible in Figs. 3a and 4a. The visualization (Fig. 3a) shows a line of separation, wrapped around the wing nose originating from a saddle point in the plane of symmetry $0.45T$ upstream of the leading edge. Separation, which occurs because of the strong adverse pressure gradient imposed by the wing in this region (Fig. 4a), allows the horseshoe vortex to form. Associated with the rotational motion of the vortex are a line of locally low wall shear stress (visible in Fig. 3a between the separation line and wing nose) and a strip of locally low wall static pressure (visible in Fig. 4a about $0.3T$ from the wing nose). Devenport and Simpson[14] demonstrate that these features lie approximately below the vortex center. Between the wing nose and maximum thickness the horseshoe vortex and surrounding boundary layer experience a strong favorable pressure gradient and substantial cross-stream gradients that, judging from the oil-flow visualization, skew the boundary layer through large angles. We would expect this skewing to turn much of the initially spanwise boundary-layer vorticity in the streamwise direction, strengthening the horseshoe vortex. Between the maximum thickness and trailing edge there is some pressure recovery that, in the oil-flow visualization, is seen to cause secondary separation. Separation lines emerge from the corner between the wing and wall at about the 88% chord location and then spread out, creating a fishtail-like pattern in the wake.

The time-dependent structure of the flow in the nose region is dominated by the bimodal unsteadiness of the horseshoe vortex. This large-scale, low-frequency unsteadiness is most clearly visible in histograms of velocity fluctuations measured in the region of leading-edge separation (Fig. 5a) that have two clearly defined peaks. It is also visible in the pressure fluctuation measurements made under the vortex to one side of the wing nose (Fig. 8a). Pressure fluctuations here are very intense, especially at low frequencies where spectral levels are nearly an order of magnitude greater than in the equivalent undisturbed boundary layer.

Some of the mean-flow structure in the wake of the baseline wing is revealed by the mean-velocity and normal-stress con-

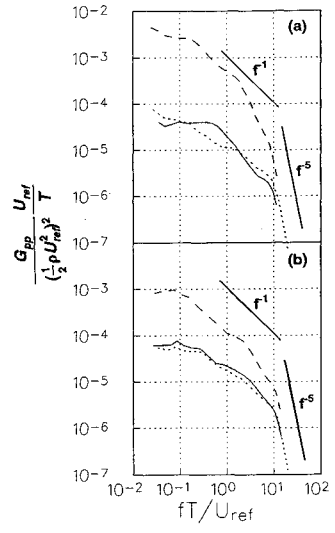


**Fig. 8 Autospectra of surface pressure fluctuations measured in the nose region at $X/T = 0.27$, $Z/T = -0.748$. Dashed line—baseline wing, solid line—wing with fillet, dotted line—undisturbed boundary layer with wing removed; a) thin boundary layer, 0-deg angle of attack; b) thick boundary layer, 0-deg angle of attack.**

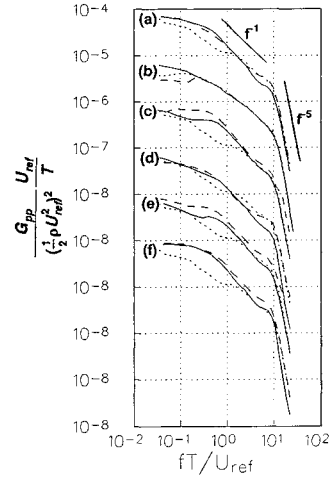


**Fig. 9 Autospectra of surface pressure fluctuations measured in the wake region at $X/T = 3$. Dashed line—baseline wing, solid line—wing with fillet, dotted line—undisturbed boundary layer with wing removed; a) thin boundary layer, 0-deg angle of attack, $Z/T = 1.28$ (baseline), $Z/T = 1.17$ (fillet); b) thick, 0 deg, $Z/T = 1.03$ (baseline), $Z/T = 1.03$ (fillet); c) thin, 6 deg, $Z/T = 2.03$ (baseline), $Z/T = 2.07$ (fillet); d) thin, 6 deg, $Z/T = -0.15$ (baseline), $Z/T = -0.04$ (fillet); e) thin, 12 deg, $Z/T = 2.97$ (baseline), $Z/T = 3.10$ (fillet); f) thin, 12 deg, $Z/T = 0.85$ (baseline), $Z/T = 0.85$ (fillet).**

tours of Figs. 6a and 7a. These contours clearly show the extent of the (horizontal) boundary layer and the (vertical) appendage wake. The streamwise legs of the horseshoe vortex are also visible through the distortion they cause to the otherwise horizontal contours of the boundary layer. Adjacent to the appendage wake, where the legs are tending to bring freestream fluid down toward the wall, mean velocities are increased and turbulence levels reduced. Both sets of contours show substantially lower boundary-layer thickness in this region than elsewhere. Farther from the wake, turbulence levels and the boundary-layer thickness are increased by the presence of the vortex. The primary cause of the higher turbulent fluctuations is not bimodal unsteadiness that, as it is currently understood, cannot occur downstream of the wing nose. Instead, it is probably additional mixing associated with the rotational motion of the vortex legs. Spanwise meandering of these legs may also contribute since the mean-velocity contours show them to be associated with significant spanwise velocity gradients in this region. Possible evidence for some large-scale motion of this type appears in the pressure spectrum measured under the vortex legs (Fig. 9a) that shows spectral levels slightly elevated above those of the undisturbed boundary layer at low frequencies ($fT/U_{ref}$ between 0.05 and 1).

### Effects of the Leading-Edge Fillet

The effects of the fillet on the flow in the vicinity of the wing nose are quite dramatic. The oil-flow visualization on the test wall (Fig. 3b) and corresponding visualizations on the fillet surface show no evidence of separation upstream of the wing. The line of low shear is also absent. Mean $U$-component velocity vectors measured close to the fillet surface in the plane of symmetry (Fig. 5) also show no evidence of flow reversal. Without leading-edge separation the bimodal unsteadiness, at least as it is currently understood, could not occur, and indeed there appears to be no evidence of it, either in the velocity histograms measured with the LDV (Fig. 5b) or in the surface pressure fluctuation spectra measured to one side of the nose (Fig. 8a). The former not only show no sign of the two peaks that characterize histograms measured with the baseline wing but also indicate peak turbulence normal stresses about an order of magnitude lower. The latter show spectral levels almost as low as in the equivalent undisturbed boundary layer.

The fillet eliminates leading-edge separation apparently by reducing the magnitude and extent of adverse pressure gradients experienced by the test-wall boundary layer upstream of the nose (Fig. 4b). Steep adverse pressure gradients are felt over a much smaller region than in the baseline case (Fig. 4a) and only close to the nose where the fillet surface is elevated above most of the boundary layer. Comparing the oil-flow streaks of Figs. 3b and 3a, it is also clear that the fillet significantly reduces the skewing of the boundary layer as it encounters the wing nose. Smaller turning angles are also implied by the surface pressure distribution (Fig. 4b) that shows much lower cross-stream pressure gradients around the wing, especially close to its maximum thickness. With less skewing we would expect less streamwise vorticity to be generated in the boundary layer.

The elimination of leading-edge separation does not necessarily imply the complete absence of the horseshoe vortex. Vortex legs, contained within open separation lines, could be formed downstream of the nose region from concentrations of skew-induced streamwise vorticity. The fact that no such separation lines are visible in Fig. 3b, suggesting either that vortex legs do not form or that they are too weak to be seen, may be a further indication of the lack of such vorticity with the fillet.

It is perhaps surprising that the fillet has almost no influence on the position of secondary separation that, in Fig. 3b, is seen to occur at about the 85% chord location. This may be a consequence of two competing factors: the virtual elimination of the horseshoe vortex and its efficient mechanism for momentum transfer to the corner between the wing and wall (hastening separation) and the reduction in the magnitude of pressure gradients around the wing, including adverse gradients in the vicinity of its trailing edge (delaying separation).

The mean-velocity and turbulence stress contours (Figs. 6b and 7b) clearly show a strong influence of the fillet on the wake. Local distortions of the contours, associated in the baseline case with the rotational motion of the horseshoe vortex legs, are greatly reduced. This at least indicates a reduction in the redistribution of streamwise momentum by the vortex legs and the nonuniformity they bring to the turbulence structure of the wake. Measurements of secondary flow velocities would be required to prove conclusively that this is a consequence of vortex legs that are much weaker or absent altogether. However, given the apparent effects of the fillet on the flow close to the wing, that seems very likely. Surprisingly,

the wall-pressure spectrum under the wake (Fig. 9a) is almost the same as in the baseline case, spectral levels being slightly elevated at low frequencies when compared with the undisturbed boundary layer.

#### Influence of Approach Boundary-Layer Thickness

The factor of two increase in approach boundary-layer thickness had surprisingly little qualitative or quantitative influence on the surface oil-flow pattern generated with the baseline wing. The location of primary separation moved from $X/T = -0.45$ to $-0.47$, and that of secondary separation from 88 to 84% chord. These small changes suggest that the size and structure of leading-edge separation and the horseshoe vortex are largely independent of surrounding boundary-layer thickness. Consistent with this, the velocity measurements made in the wake appear to show the vortex legs more deeply embedded in the thick boundary layer. A close comparison of Figs. 6a and 6c and Figs. 7a and 7c show differences in the scale and shape of the velocity contours in the vicinity of the vortex legs that are significantly smaller than those in the surrounding boundary layer. Consider, for example, boundary-layer thickness that increases by only 15% in the vicinity of the vortex legs compared with 40% in the surrounding flow. One would expect a more deeply embedded horseshoe vortex to appear more steady since on average it would mix fluid with less difference in streamwise velocity. This indeed appears to be the case; peak turbulence levels in the vicinity of the vortex legs (Fig. 7c) and spectral levels at low frequencies in the nose and wake region surface pressure spectra (Figs. 8b and 9b) are all significantly lower with the thick approach boundary layer.

The change in boundary-layer thickness appeared to have little influence on the efficacy of the leading-edge fillet. With the thick boundary layer the oil-flow visualizations showed no evidence of leading-edge separation, and LDV velocity measurements made in the nose region showed no sign of the bimodal unsteadiness. Surface pressure fluctuation spectra measured in the nose and wake region (Figs. 8b and 9b, respectively) are almost indistinguishable from those of the undisturbed boundary layer. Velocity measurements in the wake (Figs. 6d and 7d) show the fillet reducing the distortion of the wake due to the horseshoe vortex legs in much the same way, and by much the same amount, as in the thin boundary layer.

#### Influence of Angle of Attack

Apart from the expected asymmetry, placing the baseline wing at 6- and 12-deg angle of attack appeared to have little qualitative effect on its flow structure. The most significant quantitative change, observed in the oil-flow visualizations, was a slight increase in the size of the leading-edge separation. Consistent with this the surface pressure measurements showed an increase in the extent and magnitude of the adverse pressure gradients upstream of the wing nose. The pressure field changes in this way because at angle of attack the wing presents a blunter leading edge to the oncoming flow. In the wake of the baseline wing (Figs. 6e and 7e), asymmetry appears in the vortex legs. Distortions to the boundary-layer thickness and mean-velocity contours (Fig. 6e) produced by vortex leg on the pressure side (positive $Z$) of the wake appear greater than those on the suction side or at zero angle of attack. The implication is that the pressure side leg is stronger, a conjecture supported by the observation that this leg appears to have begun drawing in the otherwise vertical wake of the wing. A stronger pressure-side leg would be consistent with some of the lift on the wing model being shed at its base. Curiously, there appears to be less unsteadiness associated with the pressure side leg. Peak turbulence levels in this leg (Fig. 7e) and low- frequency surface pressure fluctuation levels underneath it (Figs. 9c and 9d) are significantly lower than on the suction side.

Overall the leading-edge fillet appears somewhat less effective with the wing at angle of attack. Although the oil-flow visualization (Fig. 3c) again shows no evidence of the type of leading-edge separation seen in the baseline case, there is some accumulation of pigment on the pressure side of the wing along a line originating in the corner between the fillet and wall. Close examination of the directions of the oil-flow streaks show them narrowly converging on this line, suggesting (as indicated in Fig. 4c) that it is an open separation. Separation may be a consequence of the locally adverse streamwise pressure gradients that appear on and close to the pressure side of the fillet at angle of attack (Fig. 4c). The general direction of the oil flow in the vicinity of the separation line suggests substantial skewing of the boundary layer and thus, presumably, an increase in its streamwise vorticity. However, this skewing is only associated with mild cross-stream pressure gradients (Fig. 4c), indicating that it may be confined to a relatively thin region adjacent to the wall. One possibility that remains to be investigated is whether or not this separation is associated with bimodal unsteadiness.

Separation appears to have a strong influence on the structure of the flow downstream of the junction. Figure 6f shows substantial distortion of the mean-velocity contours and boundary-layer thickness on the pressure side of the wake, implying the presence of an organized vortex leg here. On the suction side, however, there is little if any distortion. Consistent with this, and in contrast to the results for the baseline wing, turbulence stresses (Fig. 7f) and low-frequency surface pressure fluctuation levels (Figs. 9e and 9f) are significantly higher on the pressure than on the suction side. However, fluctuation levels and wake nonuniformity still appear less with the fillet than without.

## Conclusions

The effects of a leading-edge fillet on the flow of a turbulent boundary past an idealized appendage-body junction have been studied experimentally. The fillet consisted of a large fairing in the corner between the wing nose and the body surface upstream. Measurements made with two approach boundary layers of different thickness and with the wing at 0-, 6-, and 12-deg angle of attack suggest the following conclusions.

With the appendage at zero angle of attack in either boundary layer, the fillet 1) eliminated leading-edge separation, apparently by reducing the magnitude and extent of adverse pressure gradients experienced by the body boundary layer upstream of the nose; 2) prevented the formation of the horseshoe vortex around the appendage nose and thus eliminated its bimodal unsteadiness; 3) greatly reduced the magnitude of surface pressure fluctuations in the vicinity of the appendage; 4) reducted the magnitude of cross-stream pressure gradients in the vicinity of the appendage and thus the skewing of the boundar layer as it passed the appendage; and 5) reduced the nonuniformity of the wake associated with the horseshoe-vortex legs.

With the appendage at nonzero angle of attack, the fillet improves the characteristics of the flow. However, 6) separation of the approach boundary layer occurs along a line located on the pressure side of the fillet, apparently because of locally adverse pressure gradients here; 7) significant skewing of near-wall boundary-layer fluid occurs in the vicinity of separation; and 8) nonuniformity and unsteadiness on the pressure side of the wake is substantially greater than at zero angle of attack, suggesting the presence of a streamwise vortex here.

Overall, the leading-edge fillet appears to modify the flow past the wing-body junction in a way that would be desirable in most applications. An obvious topic for future research is the structure of the one-sided separation region produced at an angle of attack with the fillet. Whether or not this separation is associated with bimodal unsteadiness like that observed with the baseline wing remains an open question.

## Acknowledgment

This work was supported by the Office of Naval Research under Contract N00014-88-C-0291.

## References

[1]Devenport, W. J., and Simpson, R. L. "Time-Dependent and Time-Averaged Turbulence Structure Near the Nose of a Wing-Body Junction," *Journal of Fluid Mechanics,* Vol. 210, 1990, pp. 23–55.

[2]Devenport, W. J., Agarwal, N. K., Dewitz, M. B., Simpson, R. L., and Poddar, K., "Effects of a Fillet on the Flow Past a Wing-Body Junction," *AIAA Journal,* Vol. 28, No. 12, 1990, pp. 2017–2024.

[3]Kubendran, L. R., Bar-Sever, A., and Harvey, W. D., "Flow-Control in a Wing-Fuselage Type Juncture," AIAA 26th Aerospace Sciences Meeting, AIAA Paper 88-0614, Reno, NV, Jan. 1988,

[4]Sung, C.-H., Yang, C.-I., and Kubendran, L. R., "Control of a Horseshoe Vortex Juncture Flow Using Fillet," Symposium on Hydrodynamic Performance Enhancement for Marine Applications, Newport, RI, Oct. 1988.

[5]Dewitz, M. B., "The Effect of a Fillet on a Wing-Body Junction Flow," MS Thesis, Dept. of Aerospace and Ocean Engineering, Virginia Polytechnic Institute & State Univ., Blacksburg, VA, 1988.

[6]Maltby, R. L., "Flow Visualization in Wind Tunnels Using Indicators," AGARD AG 70, 1962.

[7]Sutton, E. P., Univ. of Cambridge, private communication, 1985.

[8]Devenport, W. J., and Simpson, R. L., "Some Time-Dependent Features of Turbulent Appendage-Body Juncture Flows," 16th Symposium on Naval Hydrodynamics, Berkeley, CA, July 1986.

[9]Miller, J. A., "A Simple Linearized Hot-Wire Anemometer," *Journal of Fluids Engineering,* Vol. 98, 1976, pp. 550–557.

[10]Bearman, P. W., "Corrections for the Effect of Ambient Temperature Drift on Hot-Wire Measurements in Incompressible Flow," *DISA Information,* Vol. 11, 1971, pp. 25–30.

[11]Agarwal, N. K., and Simpson, R. L. "A New Technique for Obtaining the Turbulent Pressure Spectrum from the Surface Pressure Spectrum," *Journal of Sound and Vibration,* Vol. 135, No. 2, 1989, pp. 346–350.

[12]Simpson, R. L., and Chew, Y.-T., "Measurements in Steady and Unsteady Separated Turbulent Boundary Layers," *Laser Velocimetry and Particle Sizing,* edited by H. D. Thompson and W. H. Stevenson, Hemisphere, Washington, DC, 1979, pp. 179–196.

[13]Kline, S. J., and McClintock, F. A., "Describing Uncertainties in Single Sample Experiments," *Mechanical Engineering,* Vol. 75, No. 1, 1953, pp. 3–8.

[14]Devenport, W. J., and Simpson, R. L., "The Flow Past a Wing-Body Junction—An Experimental Evaluation of Turbulence Models," *AIAA Journal,* Vol. 30, No. 4, 1992, pp. 873–881.